LUPINE PUBLISHERS

Modern Approaches on Material Science

DOI: 10.32474/MAMS.2021.03.000171

ISSN: 2641-6921

Research Article

# Annealed $Ba_{1-x}Mg_2Al_6Si_9O_{30}$:xEu Phosphors: Super-Broad Trap Level Distribution And Optical Storage Property

**Zhang X[1,2], Deng MX[1,2], Wang CY[1,2], Zheng ZH[1,3], Liu Q[1,2]*, Zhou ZZ[1] and Xu XK[1]**

[1]*The State Key Laboratory of High-Performance Ceramics and Superfine Microstructure, Shanghai Institute of Ceramics, Chinese Academy of Sciences, China*

[2]*Center of Materials Science and Optoelectronics Engineering, University of Chinese Academy of Sciences, China*

[3]*College of Materials Science and Engineering, Fuzhou University, China*

***Corresponding author:** Liu Q, The State Key Laboratory of High-Performance Ceramics and Superfine Microstructure, Shanghai Institute of Ceramics, Chinese Academy of Sciences, Shanghai 200050, China

**Received:** February 11, 2021 **Published:** February 23, 2021

## Abstract

Currently, lots of research work have been conducted to exploit inorganic optical storage materials (OSMs). Despite those impressing discoveries of new OSMs, the inducing of defects or traps and the interaction between light-emitting center and charge carrier recombination center is still under debate. Herein, through sol-gel methods, a novel $Ba_{1-x}Mg_2Al_6Si_9O_{30}$: xEu (BMASO: xEu) phosphor of OSMs was successfully synthesized. Fine crystallization of hexagonal phase was proved by XRD Rietveld refinement. From the thermoluminescence (TL) results, a super-broad distribution of trap level from 323-673 K was found for the sample BMASO:0.02Eu annealed in a reductive atmosphere, with a considerable TL intensity even in a high temperature region over 673 K. Because of the annealing in reductive atmosphere and part of Eu ions replacement for Ba or even Mg ions, many lattice defects have been caused, resulting in a large trap concentration and continuous trap distribution, which is very critical for OSMs. Finally, the potential in OSMs application was tested, showing the feasibility of photo stimulated luminescence (PSL) under laser irradiation of 980 nm and thermally stimulated luminescence (TSL) on a heating stage of 573 K, owing to the good stability and durability of the captured charge carriers in traps over 60 days in the annealed BMASO:0.02 Eu phosphor.

**Keywords:** Optical storage materials (OSMs); Trap level; Reductive annealing; Thermoluminescence; $Ba_{1-x}Mg_2Al_6Si_9O_{30}$: xEu

**Abbreviations:** BMASO:xEu: $Ba_{1-x}Mg_2Al_6Si_9O_{30}$:xEu; OSMs: Optical Storage Materials; TL: Thermo Luminescence; PSL: Photo Stimulated Luminescence; TSL: Thermally Stimulated Luminescence; PersL: Persistent Luminescence; RA: Reductive Atmosphere

## Introduction

Inorganic optical storage materials (OSMs), a kind of material which generate free charge carriers that can be captured by traps inside the lattice under the irradiation of external light with high energy. The captured charge carriers can be re-excited by light of an appropriate wavelength or heat to emit light [1-4]. The phenomenon is called photo stimulated luminescence (PSL) or thermally stimulated luminescence (TSL). While PSL or TSL were firstly observed by Boyle in early 1664, referring to the process in which materials gradually fluoresce during the heating [5]. Based on the similar mechanism of storing free charge carriers, this special trait has given rise to many functional materials in various application, for example, persistent luminescence (PersL) phosphors, X-ray storage films in medical field, radiation dosimeters and anti-counterfeiting marking materials [5-9]. Among those applications, there is one important property shared by all these materials, that is the ability to store excited charge carriers. To design and discover new materials of the same kinds, a deep understanding on the trapping process is needed.

Since Zhuang YX. et.al [10,11] discovered the surprisingly deep traps and good light responding performance in $(Sr_{1-x}Ba_x)Si_2O_2N_2$: Eu/Yb, Dy of PSL materials and demonstrated its potential application prospect on optical storage, PSL materials have begun to regain researchers' interests. Unlike previous CaS: Eu/Dy phosphor [12], silicates or oxynitrides have better stability and

are more friendly to environment, making them suitable media for OSMs applications. A lot of outstanding research work has settled on exploiting new candidates. Lin SS [13] found $BaSi_2O_5$:$Eu^{2+,}$ $Nd^{3+}$ with deep traps along with the good retention rate of information in 60 hours, as thermoluminescence (TL) test showed. The trap distribution also presented a highly concentrated trend, On this basis, Liu D et.al [9] re-excavated the $BaSi_2O_5$ substrate from an original view by introducing different doping ions to achieve multiple traps, showing us the application of OSMs in multi-dimensional information storage and encryption. Despite so many excellent works, there is still lack of basic research work on the trapping behavior of excited free carriers in traps. Thermoluminescence (TL) test is of irreplaceable role in uncovering the distribution of charge carriers in traps, which can show the variation on the intensity of emitted light as increasing the surrounding temperature.

To fully comprehend TL, there are two key parameters that should be separated, they are traps in the host lattice and light-emitting centers. Firstly, in a suitable OSM, the traps with sufficient depth are required to prevent the escape of charge carriers under normal conditions. For the light-emitting center, despite of the similar light-emitting ions shared with photoluminescence (PL), in PSL or TSL situation, it is a kind of dissipative luminescence, which requires pre-irradiation and stored carriers before it can emit light under external disturbance. Besides, after the charge carriers recombined in the recombination centers, whether their energy can be effectively transferred to the luminescent center or not is another important factor. In this work, we find that the annealed $Ba_{1-x}Mg_2Al_6Si_9O_{30}$: xEu (BMASO: xEu) phosphor has unique properties in capturing and storing excited charge carriers. As seen from TL results, this material exhibits an unusually wide distribution of trap energy levels and charge carriers trapping capabilities, including traps in deep depth which is of crucial importance in optical storage. Because its special crystal structure of BMASO: xEu, the origin of defects or traps can be ascertained to be the intrinsic lattice defects, possibly related to the oxygen vacancies caused by annealing in a reductive atmosphere (RA) rather than the effect from doping ions in other PSL materials [14-16]. To deeply reveal the influence of the crystal structural and annealing treatment on affecting the charge carriers storing behavior, systematical characterizations have been conducted and the potential in OSMs application has been tested as well.

## Experimental Work

Synthesis of BMASO: xEu Phosphors

To obtain sample $Ba_{1-x}Mg_2Al_6Si_9O_{30}$: xEu (BMASO: xEu, x =0.01, 0.015, 0.02, 0.025 and 0.03), nitric acid (AR, 65-68%), $Eu_2O_3$ (4N), $BaCO_3$ (99%), Al $(NO_3)_3 9(H_2O)$ (99.5%), Mg $(NO_3)_2$ $6(H_2O)$(99%), TEOS (0.93g/mL), polyethylene glycol and ethanol were selected and used as raw materials. Then, $Eu_2O_3$ and $BaCO_3$ were dissolved in nitric acid to obtain solution A; Mg $(NO_3)_2$ $6(H_2O)$ and Al $(NO_3)_3$ $9(H_2O)$ were dissolved in water to obtain solution B. After that, solution A and B were mixed, and placed on a magnetic stirrer. After stirring for half an hour, the solution C obtained by mixing TEOS, ethanol and polyethylene glycol (in a volume ratio of TEOS: ethanol: polyethylene glycol=5:8:20) was added to the mixed solution of A and B, and was stirred for another 3 and a half hours. Then the mixed solution was placed in a thermostat for drying to be powders, at 50 ˚C for 12 hours. The next day, the dried powders were sintered in a muffle furnace at 1300 ˚C for 5 hours in air, cooled with the furnace in air, and finally grounded into fine powders. Further, the sintered sample was placed in a tube furnace and annealed at 1300 ˚C for another 5 hours in a reductive atmosphere (RA) with Ar(95%)/$H_2$(5%) mixed gas, then cooled with the furnace, and finally grounded into fine powders.

## Characterization and Measurements

A Bruker D8 ADVANCE X-ray diffractometer (XRD) was employed to characterize phase and crystal structures using Cu K radiation at an interval of 0.02˚, ranging from 10˚ to 80˚ with a scanning speed of 5˚/min. Rietveld Refinement of the XRD profile was conducted through Fullprof software. Field emission scanning electron microscope (SEM, JSM-7800F) equipped with energy dispersive spectrometry (EDS) was used to analyze the morphology of samples. UV-visible absorption spectrum was got by SHIMADZU Model UV-2600 to investigate optical band gap of phosphors. Photoluminescence (PL) spectra and photoluminescence excitation (PLE) spectra were obtained through the fluorescence spectrophotometer (Hitachi Model F-4600, Xe lamp as light source, 150 W). Before TL measurement, a commercial Hg lamp which can emit light of wavelength on 254 and 375 nm (3 W), was applied to irradiate samples for certain time (both lights with λ=254 and 375 nm are utilized to excite the sample before every TL test), then the charged samples were sent to test after delaying for certain time in darkness. The time-dependent TL curves were recorded from 300 K (27 ˚C) to 673 K (400 ˚C) at a heating rate of 1K/s taken by a SL08 TL meter (Radiation Science and Technology Co. Ltd, Guangzhou, China). X-ray photoelectron spectrometer (XPS) data was got on AXIS Ultra in the Instrumental Analysis Center of Shanghai Jiao Tong University. PSL spectrum was collected by a FLS920 spectrometer (Edinburgh), using 980 nm laser as light source, after samples were irradiated by the commercial Hg lamp for a certain time.

## Results and Discussion

In (Figure 1a), X-ray diffraction (XRD) patterns show that phase structures of synthesized $Ba_{1-x}Mg_2Al_6Si_9O_{30}$: xEu (BMASO: xEu) all consist well with the standard card of BMASO host, PDF#83-0740, having only a small fraction of unreacted $SiO_2$. The doping of rare-earth ions Eu does not change the crystal structure. The particle size is distributed from 1-15 μm, and from EDS a uniform incorporation of all component elements is verified (Figure 1d). In (Figure 1b), Rietveld refinement is also conducted to analyze the

XRD data, taking $BaMg_2Al_6Si_9O_{30}$ as a starting model. As Table 1 shows, the reliable factors converge to Rp:10.9 and Rwp:12.7, with calculated cell parameter: a=10.1225 Å, b=10.1225 Å, c=14.3376 Å, and a direct cell volume =1272.2950 $Å^3$, indicating the refined data are in good conformity with the reflection conditions. The synthesized material is a nearly pure phase of BMASO, belonging to the hexagonal crystal system, and like the Osumilite structure, the space group is P6/mcc.

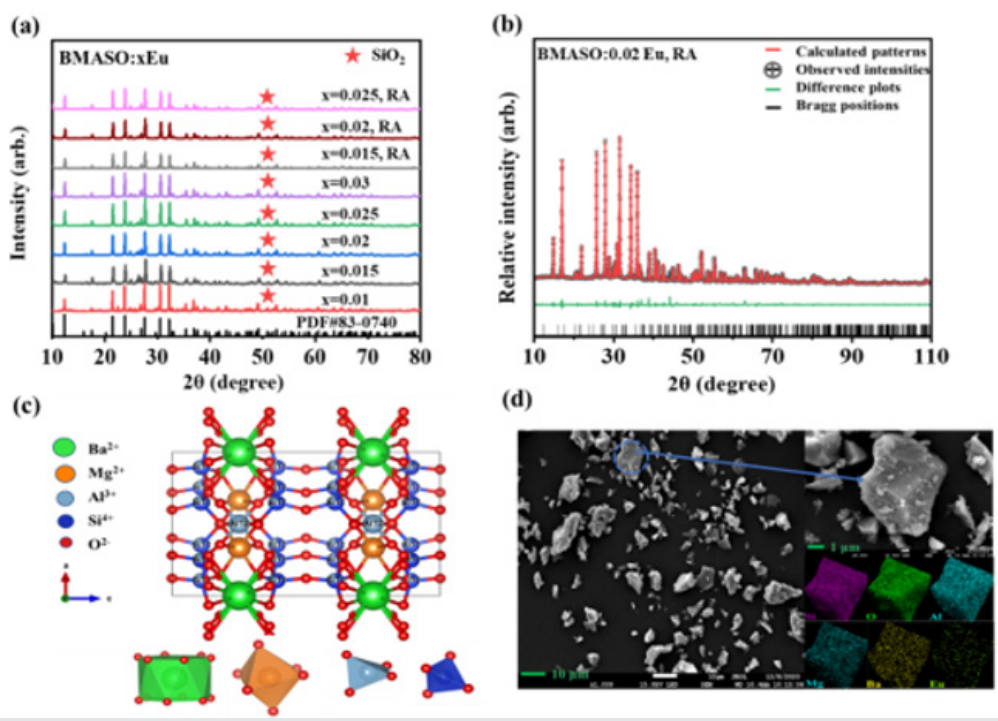


**Figure 1:** (a) XRD pattern of BMASO: xEu, sintered in air and annealed in reductive atmosphere (RA), (b) Rietveld refinement results of BMASO:0.02Eu, annealed in RA, (c) crystal structure of the host lattice, and (d) SEM images and element mapping of BMASO:0.02Eu, annealed in RA.

**Table 1:** Lattice parameters and occupation rates from Rietveld refinement for BMASO: 0.02Eu, RA.

| Atom | Site | X | Y | Z | Occupancy | U |
|---|---|---|---|---|---|---|
| BaC | 2a | 0 | 0 | 0.25 | 0.069 | 0.023 |
| MgA | 4c | 0.33333 | 0.66667 | 0.25 | 0.148 | 0.007 |
| $SiT_1$ | 24m | 0.1041 | 0.3518 | 0.10969 | 0.681 | 0.008 |
| $AlT_1$ | 24m | 0.1041 | 0.3518 | 0.10969 | 0.303 | 0.008 |
| $AlT_2$ | 6f | 0.5 | 0.5 | 0.25 | 0.237 | 0.007 |
| $O_1$ | 12l | 0.1245 | 0.4043 | 0 | 0.528 | 0.018 |
| $O_2$ | 24m | 0.2159 | 0.2835 | 0.1351 | 0.984 | 0.023 |
| $O_3$ | 24m | 0.1396 | 0.4968 | 0.1784 | 1.017 | 0.011 |
| Eu | 2a | 0 | 0 | 0.25 | 0.001 | 0.023 |
| Eu | 4c | 0.33333 | 0.66667 | 0.25 | 0.002 | 0.007 |

As (Figure 1c) and Table 1 show, unlike the referred typical cyclosilicate structure ($Si_6O_{18}$), which is composed of six silicon-oxygen tetrahedrons, the $SiO_4$ tetrahedron in the BMASO structure unit cell contains two rings, connected by six shared oxygen's ($Si_{12}O_{30}$). The two-rings unions comprise the frame of lattice and are stacked along the c-axis. Like the referred structure of Azurite, in BMASO the substitution of Al for Si has reached a maximum value, with Mg partly replacing the Al sites, and the tetrahedral occupation is divided into two types: one ($T_1$), $SiO_4$ tetrahedron, forming a double six-membered ring structure, piled along the c-axis; the other one ($T_2$), $AlO_4$ tetrahedron, located between the double six-membered rings, and sharing edges with $MgO_6$ octahedral. 12-coordinated $BaO_{12}$ are dispersed among those double six-membered rings. The sites which Eu ions are doped in are judged based on the radius similarity rule. For $Eu^{2+}$, radius is 1.17 Å, which is similar to the $Ba^{2+}$ radius of 1.61 Å, while the $Mg^{2+}$ radius is 0.72 Å. Hence, the $Eu^{2+}$ will preferentially occupy the sites of $Ba^{2+}$. As Table 1 shows, there are two chemical sites for $Eu^{2+}$, the $Ba^{2+}$ site and $Mg^{2+}$ site. This suggests that part of $Eu^{2+}$ ions can be incorporated in smaller $Mg^{2+}$ sites.

Besides crystal structure, the band gap is another important parameter for all phosphors to introduce defect levels. As the UV-Vis adsorption spectra (Figure 2) shows, using $T_{auc}$ equation (1) below, the optical band gap of BMASO can be determined as 4.6 eV, that is big enough for a broad trap level distribution.

$$\alpha h\upsilon = \beta(h\upsilon - Eg) \qquad [1]$$

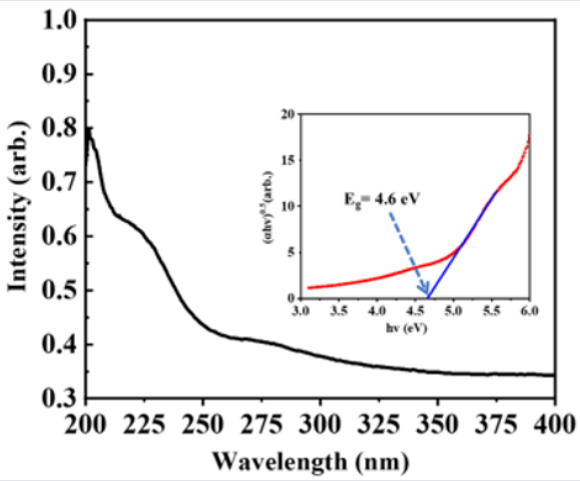


**Figure 2:** UV-Vis adsorption spectra of host material BMASO.

## Photoluminescence Properties

In (Figure 3), for samples sintered in air and annealed in RA, as the Eu doping concentration value x increases from 0.01 to 0.02, the PL and PLE intensity, excited at $\lambda_{ex}$=310 nm and monitored at $\lambda_{em}$=380 nm, rises up quickly to x=0.02 and then drops gradually when x further increases from 0.02 to 0.03, resulting from concentration quenching. Therefore, the sample with chemical composition BMASO:0.02Eu is chosen to analyze the spectrum properties more clearly, as (Figure 4) shows. In the photoluminescence excitation spectrum of BMASO:0.02Eu prepared in air, monitored at 380 nm, evident absorption peaks located at 260 nm and 310 nm can be found (Figure 4a). Under the excitation wavelength of 310 nm, the sample shows typical spectrum from $4f^65d^1$-$4f^7$ transition of $Eu^{2+}$, with an emission peak at 380 nm, and a wide bulge ranging from 400-600 nm, centered at 460 nm. Because the energy of 5d orbit is very sensitive to the surrounding crystal field, this spectrum can demonstrate the existence of two different sites occupied by $Eu^{2+}$. When switching the excitation wavelength to shorter 270 nm, some relatively low peaks at 610 nm originated from $^5D_0$-$^7F_2$ transition of $Eu^{3+}$ can be detected (inset in (Figure 4b) partly because of the decrease on the light intensity from $Eu^{2+}$ in the phosphors sintered in air. The results of the spectroscopy indicate that the samples prepared in air show a mixed valence state of $Eu^{2+}$ and $Eu^{3+}$ (inset in Figure 4b), as discovered in other aluminates and aluminosilicates [17-19]. Based on the study conducted by researchers before, there are generally four reasons for the mixed valence Eu ions when calcined in a non-reducing atmosphere [20,21].

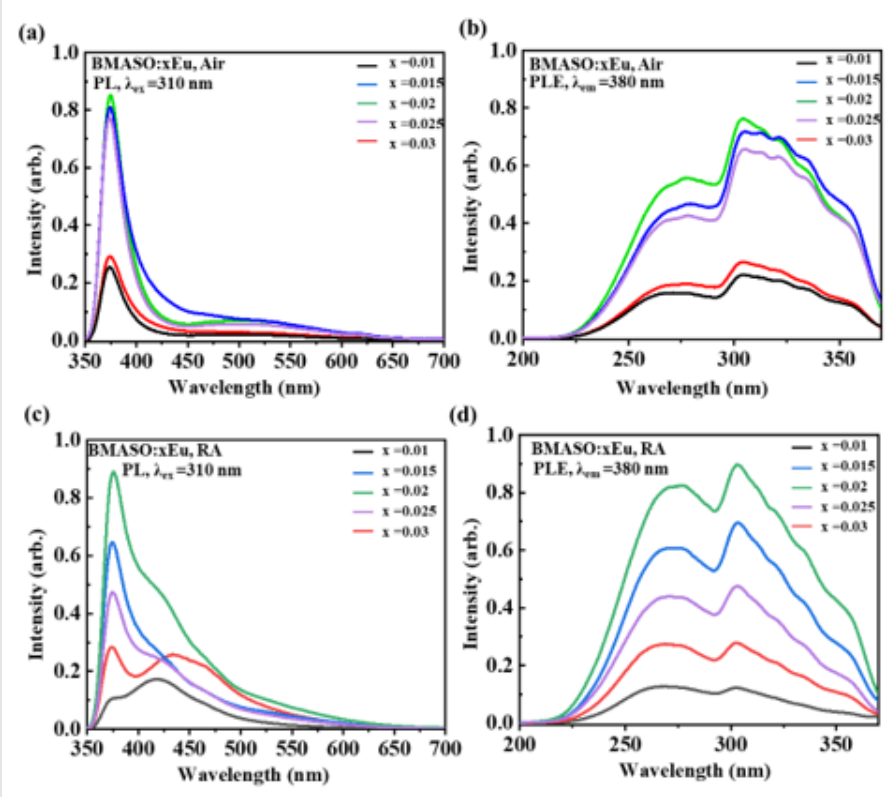


**Figure 3:** Spectra of BMASO: xEu (x=0.01, 0.015, 0.02, 0.025, 0.030) under different sintering conditions: (a) PL, $\lambda_{ex}$ = 310 nm, calcined in air, (b) PLE, $\lambda_{em}$ = 380 nm, calcined in air, (c) PL, $\lambda_{ex}$ = 310 nm, annealed in reductive atmosphere (RA), and (d) PLE, , $\lambda_{em}$ = 380 nm, annealed in RA.

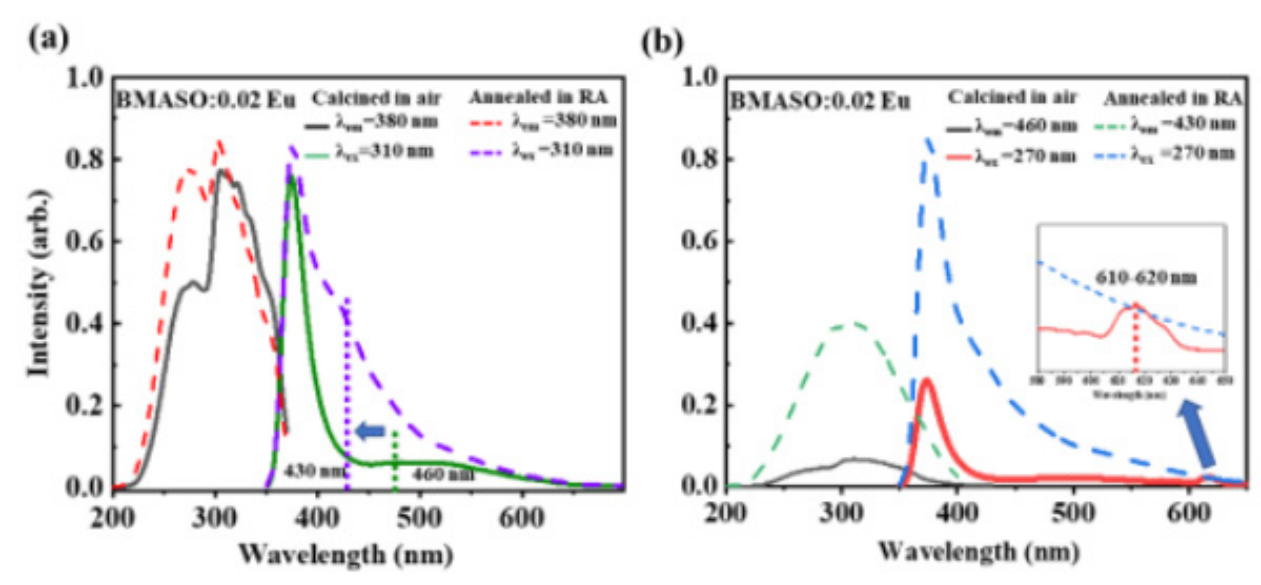


**Figure 4:** PLE and PL spectra of BMASO:0.02Eu calcined in air and annealed in RA: (a) $\lambda_{em}$ = 380 nm, $\lambda_{ex}$ = 310 nm, (b) $\lambda_{em}$ = 460 nm or 430 nm, $\lambda_{ex}$ = 270 nm.

a. There is no oxidant in the matrix lattice.

b. The ions replaced by $Eu^{3+}$ are divalent.

c. The replaced ion has a similar radius to $Eu^{2+}$

d. The substituted sites are in an appropriate environment with a fixed polyhedral structure, such as $BO_4$, $SO_4$, $PO_4$ or $AlO_4$.

Combined with the radius of different ions in BMASO lattice (the radius of $Ba^{2+}$ is 1.61 Å and radius of $Mg^{2+}$ is 0.72 Å) and the work done by Lue W et.al [22], two possible replacing sits of Eu ions can be deduced, 12-fold $Ba^{2+}$ and 6-fold $Mg^{2+}$, respectively, giving rise to the strong emission peaks at 380 nm and 460 nm from $Eu^{2+}$. Furthermore, both sites are in the stiff framework of $AlO_4$ or $SiO_4$ tetrahedrons, making it difficult for oxygen to enter and oxidize $Eu^{2+}$ to $Eu^{3+}$. At the same time, based on the theory of charge compensation, one $Eu^{3+}$ ion replacing $Mg^{2+}$ or $Ba^{2+}$ will cause charge imbalance, so electron transfer occurs, as shown in the equations (2-4) below [18], taking $Ba^{2+}$ ions as examples to illustrate the process when $Eu^{3+}$ is incorporated in the lattice.

$$3Ba^{2+} + 2E\ u^{3+} \rightarrow VBa'' + 2[Eu^{3+}]\ Ba^{\bullet} \quad (2)$$

$$VBa'' \rightarrow VB_a^{x} + 2e \quad (3)$$

$$2[Eu^{3+}]\ Ba^{\bullet} + 2e \rightarrow 2[Eu^{2+}]\ Ba \quad (4)$$

In the electron transfer process, polyhedral structure $AlO_4$ may act as an electron transferring medium [23]. The reasons above will cause the occurrence of the mixed valence state of Eu ions prepared in air. However, because the ionic radius of $Eu^{2+}$ is smaller than that of $Ba^{2+}$ , very few $O_2$ may be able to enter the crystal lattice and cause the oxidation of $Eu^{2+}$, as shown by the weak peak from 600~620 nm in the inset of (Figure 4b) of PL spectra, a typical $Eu^{3+}$ emission. After annealing in a reductive atmosphere, the characteristic emission peak of $Eu^{3+}$ in the sample totally disappears. Only the emission peaks of $Eu^{2+}$ at 390 nm and a wide bulge of 400-600 nm centered at 430 nm are found. Considering the treatment in reducing atmosphere, the most direct effect should be the lack of oxygen inside lattice. Besides, because $Ba^{2+}$ is 12-coordinated and $Mg^{2+}$ is 6-coordinated, the crystal field around $Mg^{2+}$ sites are more sensitive to oxygen loss caused under RA condition, which may lead to an obvious shift of the centered emission wavelength of the wide bulge, from 460 nm (green dash line) for the sample sintered in air to 430 nm (purple dash line) for the sample annealed in RA (Figure 4a). It can be speculated that emission band ranging from 400-600 nm, centered at 430 nm, is ascribed to the $Eu^{2+}$ at the $Mg^{2+}$ sites, while the dominant emission located at 380 nm can arise from $Eu^{2+}$ occupying $Ba^{2+}$ sites. The shapes of the spectra at 380 nm also matches well with the finding on $BaSi_2Al_2O_8$:$Eu^{2+}$, with a similar coordination environment [24]. The impact on the environment around the $Ba^{2+}$ site is relatively small when calcined in RA, so its main emission peak remains unchanged at 380 nm. To further verify the $Eu^{2+}$existence, as (Figure 5a) of XPS spectra shows, typical peaks of Eu $3d_{5/2}$ are located at the same position for the samples sintered in air and annealed in RA, with binding energy Ebinding=1136 eV, matching well with the XPS value from $3d_{5/2}$ $Eu^{2+}$ of $BaMgAl_{10}O_{17}$:$Eu^{2+}$,$Mn^{2+}$ phosphors [25]. This result indicates that the proportion of $Eu^{2+}$ does not change much after being annealed in reductive atmosphere. Combined with PL spectra, it can be deduced that divalent Eu ions occupy the largest part of Eu ions sites in powders sintered in air and verify the existence of mixed states of Eu.

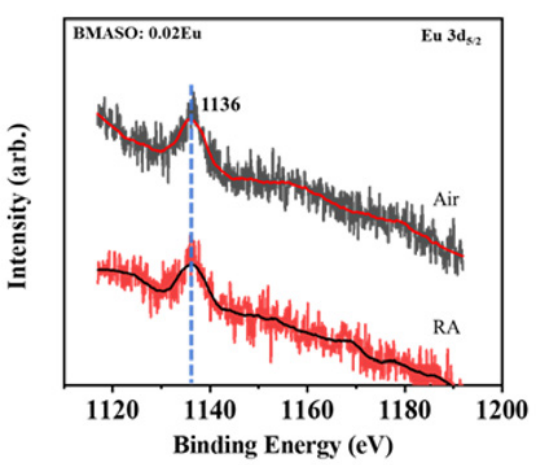


**Figure 5:** High-resolution XPS picture of Eu $3d_{5/2}$ from BMASO:0.02Eu, sintered in air and annealed in reducing atmosphere (RA).

## TL Property and Broad Trap Distribution

As illustrated in (Figure 6a), the detected thermoluminescence (TL) intensity of samples processed in air is nearly invisible as the temperature increases. However, after the phosphors are annealed in a reducing atmosphere, an obvious enhancement in TL spectra is found. Before TL test, each sample is delayed for 10 min after being irradiated by a commercial Hg lamp for 10 min at room temperature.

The TL measurement outcome can prove that the generation of defect traps is not directly related to the existence of $Eu^{2+}$, but is more closely associated with the difference in the heat treatment process. Combined with Table 2, it can be safe to claim that in this situation intrinsic defects resulting in the thermoluminescence are caused by the reductive environment treatment. From one perspective, during TL test, it is reasonable to assume that the luminescence originated from the doped Eu ions functions only as a reference for calibrating innate defects of materials. After the intrinsic traps capture free charge carriers, the captured charge carriers may recombine in situ or in other trap centers under the disturbance of external heat or light, and the energy released can be absorbed by the adjacent luminous center to emit characteristic light or depletes in other forms, the lattice vibration for instance. There are two determining points in this process: the charge carrier recombination center and the light-emitting center. Different from the TL spectra of other materials with obvious peaks, there are not several isolated and broad centralized peaks in TL curve of BMASO:0.02Eu, but an extended bulge showing a continuous distribution of trap levels. The intensity begins to rise from 373 K, reaches the top at 473 K, and then slowly drops down until 623 K. Finally, a plateau appears at 623 K and slowly extends to 673 K. This trait indicates that the defects energy levels of the traps within the phosphors present a high degree of correlation, but not a relatively concentrated distribution in other optical storage materials.

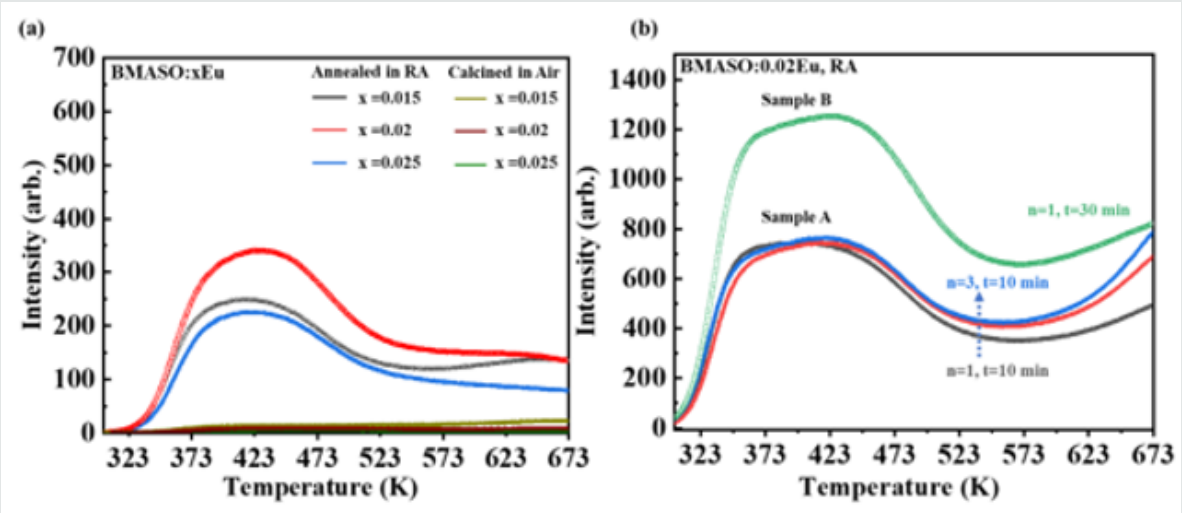


**Figure 6:** (a) TL glow curves of samples BMASO: xEu sintered in air and annealed in reducing atmosphere, x=0.015, 0.02, 0.025. (b) TL glow curves of Sample A and B with different circle times (n) and duration time (t) for BMASO: 0.02Eu, RA.

**Table 2:** PL and TL property comparison for samples experienced different atmosphere treatment.

| Sample | Sintering environment | PL spectra | TL spectra |
|---|---|---|---|
| BMASO:0.02Eu | Sintered in air | Strong emission of $Eu^{2+}$ and weak emission of $Eu^{3+}$ | No signal |
| BMASO:0.02Eu | Annealed in RA | Typical emission band from $Eu^{2+}$ | Strong signal |
| BMASO | Sintered in air or annealed in RA | No intensity | No signal |

Subsequently, to get the relationship between the filling behavior of free charge carriers and the excitation duration in TL measurement processing, as (Figure 6b) shows, two samples, A and B, of the same composition BMASO:0.02Eu, RA are applied. In (Figure 6b), n refers to the measuring circle times, while t means the duration of irradiation time. In each circle, the sample is irradiated using a commercial Hg lamp for 10 minutes (t=10 min), delayed for 10 minutes in darkness, and then subjected to TL test, in a range of 273-673 K. Sample A undergoes three circles continuously (n=3), while Sample B only undergoes once with a longer duration time for 30 minutes (t=30 min). Comparing two TL curves, it can be found that the TL intensity in the high-temperature zone (over 673 K) is gradually increasing, mainly because the environment of temperature from 273-673 K cannot supply enough energy to unlock trapped charge carriers in higher temperature zone. Also, the intensity of light between 323-423 K or 423-523 K regions remains the same in each circle for Sample A. Nonetheless, the TL intensity of Sample A at 673 K in the last circle is nearly equal to that of Sample B, indicating the existence of charge carrier's accumulation in traps of deeper depth. To deeply unearth the distribution of trap depth, the initial rise method is applied. This method has been applied to figure out the distribution of traps in many works [26,27]. Selecting BMASO:0.02Eu as a represent, in each circle the sample is placed on the heating stage with different temperature ($T_{ex}$) and charged by a commercial lamp for 1 min, then delayed in darkness at room temperature for 3 min, finally subjected to TL test from 293-673 K to plot the curves in (Figure 7b).

Because when the temperature is high enough, the detrapped charge carriers responsible for the emitting light will be reduced for the competition with lattice thermal vibration. So, the thermal quenching spectra of PL is used as a reference to calibrate the amounts of trapped charge carriers in high temperature region. The luminous intensity of PL can still maintain a high intensity at high temperatures (Figure 7a). When temperature reaches 563 K, the light keeps 67% of the original intensity (inset in Figure 7a). All data applied to initial rise method has been corrected by thermal quenching curve except for the part over 573 K since the temperature limitation is 573 K in PL test. Using the equation (5) below to identify the trap depth, the TL glow curve is plotted as ln(I) versus 1/T, and the distribution traps depth, ranging from 0.62 eV to 1.32 eV, exhibits a wide extension, as indicated in (Figure 7c-d).

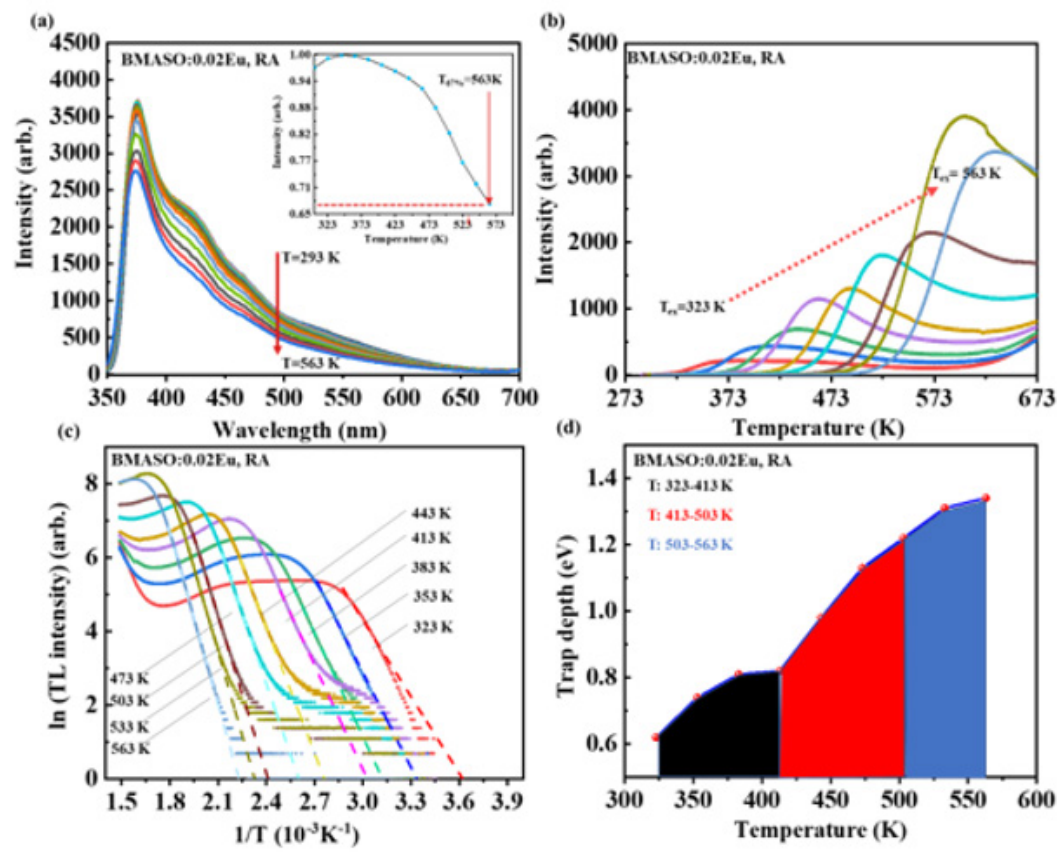


**Figure 7:** (a) Temperature dependent PL spectra from 293 K to 563 K, $\lambda_{ex}$=310 nm, BMASO:0.02Eu, RA. Trap distribution in BMASO:0.02Eu, RA: (b) TL glow curves after being irradiated at different temperature ($T_{ex}$) within 1 min; (c) initial rise plotting of TL glow curves using the data from graph (b), the slope of curve is directly related to the trap depth; (d) distribution of traps of different depth in varying temperature.

$$I(T) = C_{exp}(\frac{-ET}{kT}) \quad (5)$$

Surprisingly, it is found that the trap capturing process is thermally activated. Since as the experimental temperature Tex increases, TL intensity in higher temperature region adds up quickly (Figure 7b), in the same charging duration and delaying time. This means there are more charge carriers being locked in traps of deeper depth when Tex increases. These properties show some similarities to TL performance of $SrAl_2O_4$:Eu,Dy from 193-273 K. In that work, the blue light can be only observed at temperature at 273 K (0 ˚C), while the green light is still evident at higher room temperature [28]. More importantly, this thermally activated phenomenon at high temperatures, as BMASO:0.02Eu shows, may facilitate the search for PersL materials with proper Toptimum matched with their working conditions [29].

This unique property of TL intensity increases at higher temperatures in BMASO:0.02Eu, RA can get explained from $Eu^{2+}$ ion doping environment. The doping sites of $Eu^{2+}$, both $Mg^{2+}$ and $Ba^{2+}$ sites, are all enclosed by $AlO_4$ or $SiO_4$ stiff tetrahedron. Consequently, the secondly-generated free charge carriers excited by exterior ultraviolet light, which are firstly captured by the oxygen vacancies arising from annealing at RA, can be directly re-captured by $Eu^{2+}$ after being exposed to external heating or perturbation of light with suitable wavelength, leading to the characteristic lighting of $Eu^{2+}$. During the process, as $Eu^{2+}$ is closely coordinated with the surrounding oxygen vacancy defects, it can cut down extra energy loss caused by lattice vibration. That means it can accurately reflect the defects distribution in the lattice. This continuous curve in TL is exactly the real reflection of the continuous defect trap energy levels in the crystal lattice of the inorganic compound. Although, as shown in the work of Wang CL et al. [3], the peaks of Tl are very centralized, in inorganic compounds just like the description of Van den Eeckhout, it is unreasonable to assume that the traps are discretely distributed, because of the randomness in the bond length and bond angle of the ions around the trap center [30]. In addition, the distance between the trap centers and the light-emitting centers will also influence the accuracy of the trap depth calculated from the TL graph. As for the unusual trend of TL in high temperature region over 573 K, it was pointed out in the work of Liu BT et al. [31], in the mixed states of $Eu^{2+}$/ $Eu^{3+}$ that $AlO_4$ unions play a crucial role in transporting electrons in the compound with mixed valence state of Eu, which may account for why BMASO: xEu still has high TL intensity in the high temperature section. Because when the temperature rises to a certain level, the fluorescence will suffer from thermal quenching effect due to energy loss through the intense lattice vibration at high temperatures, instead of being released in the form of light. However, in BMASO:0.02Eu, compared with other materials, the escaped free charge carriers are effectively transferred to the luminescent center through $AlO_4$ unions, relieving energy consumption induced by thermal vibration at high temperature.

## Optical Storage and Durability

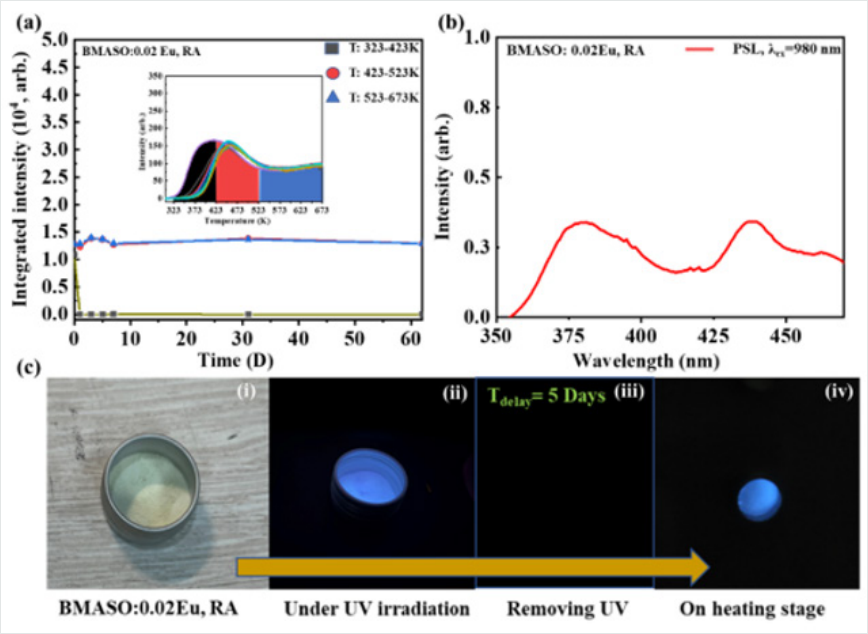


**Figure 8:** (a) Curves of delaying time dependent TL integrated intensity in three different temperature regions (black, red, blue), based on TL spectra of BMASO: 0.02Eu, RA in the inset. (b) PSL spectrum of BMASO: 0.02Eu, RA, under excitation of 980 nm laser. (c) Images of BMASO:0.02Eu, RA phosphors (i); emitting under UV irradiation for 5 mins (ii); 5 days' delaying in darkness (iii); and then emitting light again on a heating stage at 573 K, that is TSL (iv).

There is very few work on the stability of trapped charge carriers over one month, though some equations have been employed in estimating the rough years [30]. To figure out the storing ability over long time delaying, the integrated intensity of TL is plotted against the delaying time, choosing BMASO:0.02 Eu as the sample. After irradiated by UV light from a commercial Hg lamp for 10 min, powders are delayed for different time before being subjected to TL test. From the (Figure 8a), it can be found that charge carriers in traps distributed in higher 423-523 K and 523-673 K region are quite stable even after 2 month-delaying. On the contrary, the charge carriers located in shallower traps ranging from 323-423 K depleted quickly in one day. To verify the optical storage property, PSL spectrum was measured by stimulation of a 980 nm laser, pre-excited using a commercial Hg lamp. As depicted in (Figure 8b), PSL spectrum shows a strong and wide emission in the range of 350-475 nm. (Figure 8c) shows that the visualized thermal stimulated luminescence (TSL) process of charged BMASO:0.02Eu phosphors by heating powders on a heating stage to 573 K, after being delayed for 5 days in darkness. The presented optical storage ability and its durability makes BMASO:0.02Eu phosphors possess an enormous potential application in luminescence (PersL) phosphors, X-ray storage films in medical field, radiation dosimeters, and anti-counterfeiting marking materials.

## Conclusion

In summary, BMASO:xEu phosphors were synthesized by sol-gel method. Combining the TL results of samples sintered in air and annealed in reductive atmosphere (RA), it is safe to claim the origin of defects in BMASO:0.02Eu, leading to the emitted light of TL as increasing temperature, should be mainly the oxygen vacancies inside the host lattice resulting from reductive annealing. Furthermore, using the initial rise method, the trap depth shows a super-broad distribution ranging from 0.62 to 1.32 eV. To better comprehend the extremely wide trap distribution and thermally activated charging characteristics of BMASO:0.02Eu (RA) on TL test, the TL curve is divided into three parts, 323-423 K, 423-523 K and 523-673 K and it has be found that charge carriers in traps distributed in higher 423-523 K and 523-673 K region are quite stable even after 2 month-delaying, on the contrary, the charge carriers located in shallower traps ranging from 323-423 K depleted quickly in one day. The delaying time dependent TL integrated intensity indicate the durability of captured carriers in traps in high temperature region. Besides, the potential as an optical storage material for BMASO:0.02Eu (RA) is also successfully demonstrated using PSL spectrum and TSL experimental photographs.

## Acknowledgements

Many thanks for the financial supports from the National Key Research and Development Program of China (Grant No. 2018YFB0704103) and the Natural Science Foundation of Shanghai (Grant No. 20ZR1465900).

## References

1. Lin SS, Lin H, Ma CG, Cheng Y, Ye S, et al. (2020) High-security-level multi-dimensional optical storage medium: nanostructured glass embedded with $LiGa5O_8:Mn^{2+}$ with photostimulated luminescence. Light-Sci Appl 9(1): 2047-7538.
2. Wang WX, Yang JX, Zou ZH, Zhang JC,Li H, et al. (2018) An isolated deep-trap phosphor for optical data storage. Ceram Int 44(8): 10010-10014.
3. Wang CL, Jin Y H, Lv Y, Ju GF, Liu D, et al. (2018) Trap distribution tailoring guided design of super-long-persistent phosphor $Ba_2SiO_4:Eu^{2+,}$ $Ho^{3+}$ and photostimulable luminescence for optical information storage. J Mater Chem C 6(22): 6058-6067.
4. Wang B, Li XS, Chen YQ, Chen Y, Zhou J, et al. (2018) Long persistent and photo-stimulated luminescence in $Pr^{3+}$-doped layered perovskite phosphor for optical data storage. J Am Ceram Soc 101(10): 4598-4607.
5. Salis M (2003) On the photo-stimulated luminescence of $BaFBr:Eu^{2+}$ phosphors. J Lumin 104(1-2): 17-25.
6. Kato K, Tsutai I, Kamimura T, Kaneko F, Shinbo K, et al. (1999) Thermoluminescence properties of $SrAl_2O_4$: Eu sputtered films with long phosphorescence. J Lumin 82(3): 213-220.
7. Vonseggern H, Voigt T, Knupfer W, Lange G (1988) Physical model of photostimulated luminescence of x-ray-irradiated $BaFBr^-Eu^{2+.}$ J Appl Phys 64(3): 1405-1412.
8. Yamaga M, Tanii Y, Kodama N, Takahashi T, Honda M (2002) Mechanism of long-lasting phosphorescence process of $Ce^{3+}$-doped $Ca_2Al_2SiO_7$ melilite crystals. Phys Rev B 65(23): 1098-0121.
9. Liu D, Yuan LF, Jin YH, Wu HY, Xiong G, et al. (2019) Tailoring multidimensional traps for rewritable multilevel optical data storage. ACS Appl Mater Interfaces 11(38): 35023-35029.
10. Zhuang YX, Lv Y, Wang L, Chen WW, Zhou TL, et al. (2018) Trap depth engineering of $SrSi_2O_2N_2:Ln^{(2+),}$ $ln^{(3+)}$ ($Ln^{(2+)}$=Yb, Eu; $ln^{(3+)}$=Dy, Ho, Er) persistent luminescence materials for information storage applications. ACS Appl Mater Interfaces 10(2): 1854-1864.
11. Zhuang YX, Wang L, Lv Y, Zhou TL, Xie R (2018) Optical data storage and multicolor emission readout on flexible films using deep-trap persistent luminescence materials. Adv Funct Mater 28(8): 1705769.
12. Burbano DCR, Rodriguez EM, Dorenbos P, Bettinelli M, John AC (2014) The near-IR photo-stimulated luminescence of $CaS:Eu^{2+}/Dy^{3+}$ nanophosphors. J Mater Chem C 2(2): 228-231.
13. Lin SS, Lin H, Huang QM, Cheng Y, Wang J, et al. (2019) A photostimulated $BaSi_2O_5:Eu^{2+}$, $Nd^{3+}$ phosphor-in-glass for erasable-rewritable optical storage medium. Laser & Photonics Rev 13(4): 11.
14. Li M, Yu X, Xu XH, Cheng S, Zhang B, et al. (2015) Color variation between PSL and PL in $CaAl_2Si_2O_8:Tb^{3+}$ with the assistance of trap level. J Am Ceram Soc 98(7): 2008-2010.
15. Li Y, Zhou SF, Li YY, Sharafudeen K, Ma Z, et al. (2014) Long persistent and photo-stimulated luminescence in $Cr^{3+}$-doped Zn-Ga-Sn-O phosphors for deep and reproducible tissue imaging. J Mater Chem C 2(15): 2657-2663.
16. Chen DQ, Zhou Y, Xu W, Zhong JS, Huang P (2016) Persistent and photo-stimulated luminescence in $Ce^{3+}/Cr^{3+}$ activated $Y_3Al_2Ga_3O_{12}$ phosphors and transparent phosphor-in-glass. J Mater Chem C 4(48): 11457-11464.
17. Guo H, Liu XY, Li F, Wei RF, Wei Y, et al. (2012) Enhanced white luminescence in mixed-valence Eu-doped $BaAl_2Si_2O_8$ glass ceramics for W-LEDs. J Electrochem Soc 159(6): J223-J226.
18. Chen J, Liu YG, Liu HK, Ding H, Huang Z (2015) Tunable $SrAl_2Si_2O_8:Eu$ phosphor prepared in air via valence state-controlled means. Opt Mater 42: 80-86.
19. Peng MY, Hong GY (2007) Reduction from $Eu^{3+}$ to $Eu^{2+}$ in $BaAl_2O_4:Eu$ phosphor prepared in an oxidizing atmosphere and luminescent properties of $BaAl_2O_4:Eu$. J Lumin 127(2): 735-740.

20. Peng MY, Pei ZW, Hong GY, Su Q (2003) The reduction of $Eu^{3+}$ to $Eu^{2+}$ in $BaMgSiO_4$:Eu prepared in air and the luminescence of $BaMgSiO_4$:$Eu^{2+}$ phosphor. J Mater Chem 13(5): 1202-1205.

21. Xue J, Song MJ, Noh HM, Park SH, Choi BC, et al. (2020) Achieving non-contact optical thermometer via inherently $Eu^{2+}$/$Eu^{3+}$-activated $SrAl_2Si_2O_8$ phosphors prepared in air. J Alloy Compd 843: 10.

22. Lue W, Hao ZD, Zhang X, Luo YS, Wang SJ, et al. (2011) Tunable full-color emitting $BaMg_2Al_6Si_9O_{30}$:$Eu^{2+}$, $Tb^{3+}$, $Mn^{2+}$ phosphors based on energy transfer. Inorg Chem 50(16): 7846-7851.

23. Pei ZW, Zeng QH, Su QA (2000) The application and a substitution defect model for $Eu^{3+}$--$Eu^{2+}$ reduction in non-reducing atmospheres in borates containing $BO_4$ anion groups. J Phys Chem Solids 61(1): 9-12.

24. Im WB, Kim YIDY (2006) Thermal stability study of $BaAl_2Si_2O_8$:$Eu^{2+}$ phosphor using its polymorphism for plasma display panel application. Chem Mater 18(5): 1190-1195.

25. Zhang JC, Zhou MJ, Liu BT, Wen Y, Wang Y (2012) The ultraviolet irradiation degradation of fluorescent lamp used $BaMgAl_{10}O_{17}$:$Eu^{2+}$,$Mn^{2+}$ phosphor. J Lumin 132(8): 1949-1952.

26. Wang B, Lin H, Xu J, Chen H, Zebin L, et al. (2015) Design, preparation, and characterization of a novel red long-persistent perovskite phosphor: $Ca_3Ti_2O_7$:$Pr^{3+}$. Inorg Chem 54(23): 11299-11306.

27. Wang ZB, Wang WX, Zhou H, Zhang JC, Peng S, et al. (2016) Superlong and color-tunable red persistent luminescence and photostimulated luminescence properties of $NaCa_2GeO_4F$:$Mn^{2+}$,$Yb^{3+}$ phosphor. Inorg Chem 55(24): 12822-12831.

28. Botterman J, Joos JJ, Smet PF (2014) Trapping and detrapping in $SrAl_2O_4$:Eu,Dy persistent phosphors: influence of excitation wavelength and temperature. Phys Rev B 90(8): 15.

29. Du JR, Feng A, Poelman D (2020) Temperature dependency of trap-controlled persistent luminescence. Laser & Photonics Rev 14(8): 9.

30. Van Den EK, Bos A JJ, Poelman D, Smet PF (2013) Revealing trap depth distributions in persistent phosphors. Phys Rev B 87(4): 045126.

31. Liu BT, Wang YH, Zhou J, Zhang F, Wang Z (2009) The reduction of $Eu^{3+}$ to $Eu^{2+}$ in $BaMgAl_{10}O_{17}$:Eu and the photoluminescence properties of $BaMgAl_{10}O_{17}$:$Eu^{2+}$ phosphor. J Appl Phys 106(5): 053102.



**DOI:** 10.32474/MAMS.2021.03.000171